

Lawrence Berkeley National Laboratory

Recent Work

Title

Sensitivity of CO2 migration estimation on reservoir temperature and pressure uncertainty

Permalink

<https://escholarship.org/uc/item/1f24m99s>

Journal

Energy Procedia, 1(1)

ISSN

1876-6102

Authors

Jordan, P
Doughty, C

Publication Date

2009-02-01

DOI

10.1016/j.egypro.2009.02.055

Peer reviewed

GHGT-9

Sensitivity of CO₂ migration estimation on reservoir temperature and pressure uncertainty

Preston Jordan^{a*} and Christine Doughty^a

^a*Lawrence Berkeley National Laboratory, 1 Cyclotron Road MS90-1116, Berkeley, CA 94706 USA*

Elsevier use only: Received date here; revised date here; accepted date here

Abstract

The density and viscosity of supercritical CO₂ are sensitive to pressure and temperature (PT) while the viscosity of brine is sensitive primarily to temperature. Oil field PT data in the vicinity of WESTCARB's Phase III injection pilot test site in the southern San Joaquin Valley, California, show a range of PT values, indicating either PT uncertainty or variability. Numerical simulation results across the range of likely PT indicate brine viscosity variation causes virtually no difference in plume evolution and final size, but CO₂ density variation causes a large difference. Relative ultimate plume size is almost directly proportional to the relative difference in brine and CO₂ density (buoyancy flow). The majority of the difference in plume size occurs during and shortly after the cessation of injection.

© 2008 Elsevier B.V. All rights reserved

Keywords: geologic carbon storage, pressure temperature sensitivity, buoyancy-driven flow

*Corresponding author. Tel.: 00 1 510 486-6774; fax: 00 1 510 486-5686.
E-mail address: pdjordan@lbl.gov.

1. Introduction

Geological carbon sequestration (GCS) is an emerging set of technologies for storing carbon dioxide (CO₂) from point emission sources in geologic materials in the subsurface. Currently, the majority of the storage capacity identified in the subsurface consists of porous rocks saturated with brine (water too salty for human use without treatment). GCS in these so-called “brine reservoirs” involves injection of CO₂ that primarily displaces the brine in the short term, but also dissolves into it to some extent. The density of CO₂ is less than that of brine at pressure and temperature (PT) combinations common in the non-marine continental subsurface making buoyancy-driven flow potentially important. Carbon dioxide density is quite sensitive to PT, while brine density is not. Consequently, buoyancy-driven flow of CO₂ in brine is primarily dependent on CO₂ density. Brine viscosity is sensitive primarily to temperature.

Both brine viscosity, CO₂ viscosity, and the brine/CO₂ density difference are thought to be fundamental factors in CO₂ plume evolution given a particular geologic setting [1]. For brine of a given salinity, these parameters are largely dependent on PT of a particular reservoir. Reservoir PT can be uncertain due to the limits of measurement technology or variability within a reservoir. Such was observed in initial oil-field PT data in the vicinity of WESTCARB’s upcoming Phase III pilot test injection site at Kimberlina in the southern San Joaquin Valley in California. This paper presents the results of research into the probability distribution of PT conditions at this site, and explores the sensitivity of CO₂ plume evolution and final size to different PTs within this distribution through numerical simulations. These results indicate that variation in CO₂ density is the critical parameter relative to PT uncertainty/variation while brine viscosity differences have virtually no impact (CO₂ viscosity is strongly correlated to CO₂ density, so it is not considered as an independent parameter). Relative CO₂ plume size at different PTs is almost directly proportional to the relative CO₂–brine density difference. The majority of the difference in plume size due to different PTs typically occurs during injection.

2. PT probabilities at Kimberlina

Initial PTs are reported for the numerous oil and gas fields in the vicinity of the Kimberlina site in DOGGR [2]. Figure 1 shows a plot of these PTs with respect to depth. From these plots the average surface temperature is estimated as 23° C (74° F) and the average water table depth as 100 m (330 ft). These constants allowed conversion of each PT value into a pressure gradient relative to hydrostatic and a geothermal gradient.

a)

b)

Figure 1. Initial a) pressures and b) temperatures in oil and gas reservoirs near the Kimberlina site.

Figure 2 shows the geothermal gradient plotted against the pressure gradient. The linear regression indicates there is no correlation between the two. Taken separately, these gradients are normally distributed. Figure 3 shows possible PT conditions based on all combinations of the mean, $+2\sigma$, and -2σ pressure and temperature gradients with depth. The symmetric interval containing 95% of the probable PT conditions is also shown.

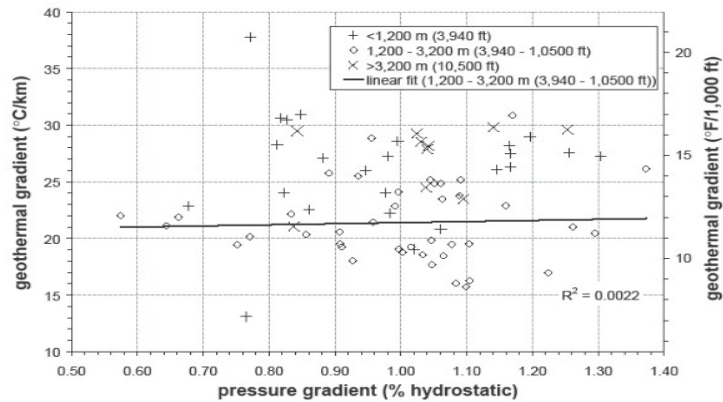


Figure 2. Geothermal gradients from initial reservoir temperatures plotted against pressure gradients from initial reservoir pressures in the vicinity of the Kimberlina site.

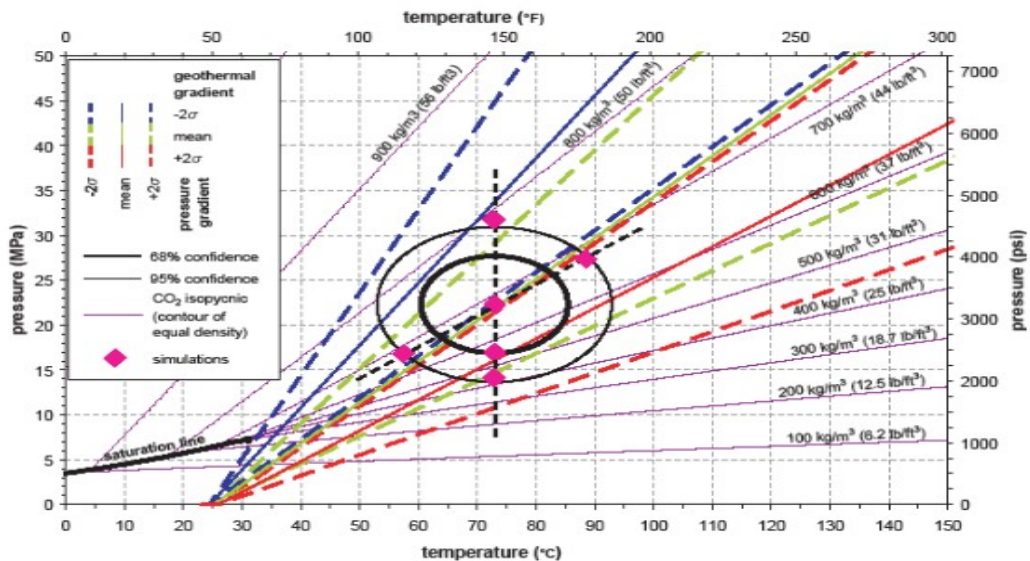


Figure 3. Range of PT probabilities at the Kimberlina site. Red, green, and blue lines show profiles of pressure versus temperature for all combinations of the mean and $\pm 2\sigma$ gradient of each parameter versus depth. Simulation cases are indicated. These are arranged along lines of constant CO₂ density (sloping black dashed line) and brine viscosity (vertical black dashed line) passing through the centroid of the probability distribution.

3. Kimberlina Phase III Pilot Test Numerical Simulation Background

WESTCARB's phase III pilot test will consist of the injection of 250,000 metric tonnes (275,500 tons) per year of CO₂ for four years. The CO₂ will be injected into the Vedder Formation at a depth of approximately 2,200 meters (7,200 feet). The lower Miocene Vedder Formation consists of marine sediments averaging 160 m (520 ft) thick in the vicinity of the site. The Vedder Formation consists of sandstones interlayered with shale. The sandstones generally comprise 50% of the formation thickness.

The Vedder Formation is overlain by the lower Miocene Freeman-Jewett Formation. This 180 m (590 ft) thick unit is a marine shale and siltstone with thin sandstone beds. It is regionally extensive and is believed to provide a continuous seal over the Vedder Formation.

The injection was numerically simulated using the ECO2 equation of state package of TOUGH2 [3,4]. This code incorporates hysteretic formulation for capillary pressure and relative permeability [5], allows for salt precipitation and dissolution, but does not account for fluid-rock chemical reactions. While the code can account for non-isothermal conditions, for computational efficiency during this study a constant reservoir temperature was imposed.

The model grid extends 8 km (5 mi.) in the four principal directions from the injection site. The Vedder Formation is modeled at a constant thickness with a uniform dip of 7° S60W. Simulations without dip were also run for comparison.

The grid cells are 5 m (16.4 ft) square at the injection well grading to a maximum 50 m (164 ft) square within the approximately 2 km (1.24 mi.) distance from the injection site anticipated to contain the plume. The grid cell size gradually increases farther away. The east-west model boundaries are constant pressure and the north-south model boundaries are no-flow (these boundary conditions do not reflect actual geological structure, but are chosen for numerical convenience; models using all constant-pressure or all no-flow boundaries showed that the evolution of the CO₂ plume is not sensitive to the lateral boundary conditions, since they are so far away from the CO₂ plume itself). Vertically, the grid consists of 30 layers, which affords at least two layers per sandstone bed. The top and bottom of the model are no-flow boundaries, representing the overlying Freeman-Jewett shale as well as underlying fine-grained continental deposits.

In the model, injection is distributed into each sandstone in proportion to its thickness. This biases injection into deeper layers relative to what would occur in a single, conventional vertical injection well, but is consistent with injection from a multi-zone well with independent pressure control at each zone. The sandstone and shale properties are as shown in Table 1. The brine salinity was taken as 50,000 ppm. Subsequent plots of oil field data indicate the salinity in the Vedder is probably closer to 20,000, but this is unlikely to significantly change the evolution of the modeled plumes, particularly with regard to relative comparisons between them.

Table 1. Numerical simulation parameters.

Facies	Porosity	Horizontal permeability	Vertical permeability	Residual liquid saturation	Maximum residual gas saturation
sandstone	28%	200 mD	20 mD	0.2	0.28
shale	15%	0.1 mD	0.01 mD	0.3	0.29

4. Kimberlina Phase III Pilot Test Numerical Simulation PT Case Selection

Figure 3 shows the PT cases considered for numerical simulations of the Kimberlina CO₂ injection. One case lies at the centroid of the PT probability space. Outlying cases are selected at PTs resulting in the same CO₂ density as the centroid and at PTs resulting in the same brine viscosity as the centroid. The latter are simply taken as occurring at different pressures and the same temperature. While this does not yield exactly the same brine viscosity across these cases, the variation with pressure is sufficiently small as to be ignored for the purposes of this study.

The outlying cases relative to the PT centroid were selected at approximately the 95% confidence limits for CO₂ density along the constant brine viscosity axis and approximately the 95% confidence limit for brine viscosity along the constant CO₂ density axis. This results in a PT outside the 95% PT interval for the high CO₂ density case along the constant brine viscosity axis. This density is at the 95% limit of CO₂ density probability, however, as these densities occur within the 95% PT interval at lower PT.

5. Results

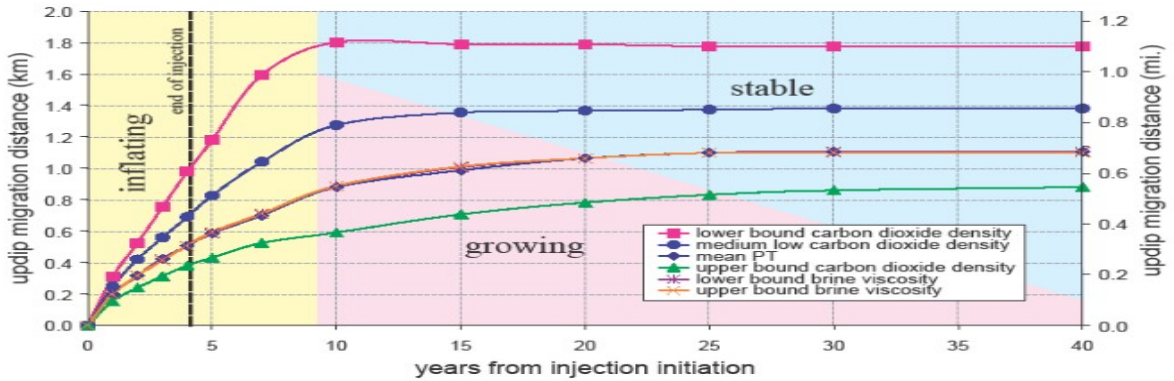
A plan view of the simulation results at the PT centroid is shown on Figure 4. Note the injection results in stacked plumes in the Vedder Formation due to the sandstone and shale interbedding and the injection into all sandstones in the Vedder. Figure 4 shows only the most extensive plume at each time step. Note the grid artifacts during injection due to the north-south, east-west rectilinear grid.

Figure 5 shows the simulated updip migration distances from the injection well for the dipping cases. Figure 6 shows the average migration distances for the flat cases. Migration distance was considered the distance from the injection well to the 5% saturation contour. This saturation was selected because lower saturation contours are subject to greater numerical effects.

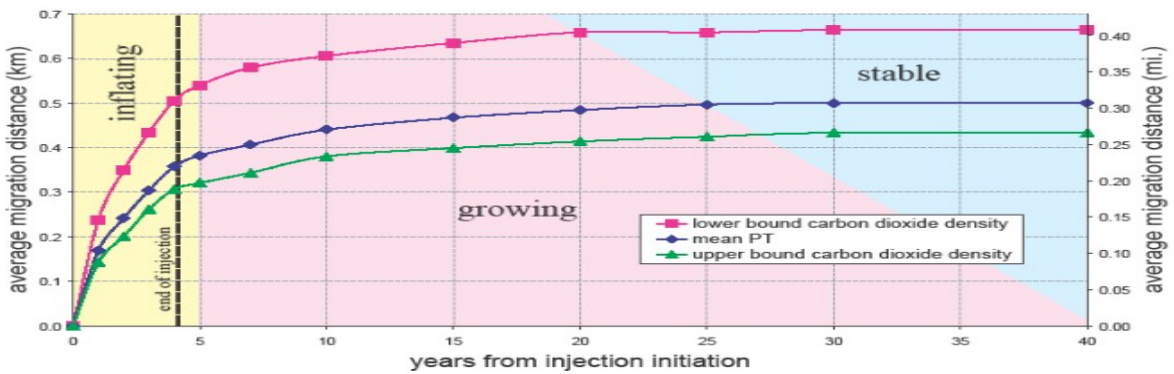
Figure 4. Extent of numerically simulated supercritical phase CO₂ from the Kimberlina injection at the centroid PT.

6. Discussion

As shown on Figure 5, the CO₂ migration distance is quite sensitive to CO₂ density, but not at all sensitive to the expected variation in brine viscosity across the probable range of PTs. The migration distance varies by a factor of two across probable CO₂ densities, but varies by so little across the probable brine viscosities that these results plot essentially on top of each other (brine viscosity variation cases were not run for the no dip scenarios based upon the results from the dipping scenarios). Conversely, plume stability is reached more quickly with the greater migration distances caused by lower CO₂ densities, particularly for the dipping strata cases. For these, plume stability was achieved in a third the time for the lowest as compared to the highest density case.



a)



b)

Figure 5. Migration distance of supercritical CO₂: a) maximum updip for dipping cases and b) average for flat cases.

Figure 5 indicates that the absolute difference in migration distance resulting from different PTs reaches about half or more of the ultimate difference by the time injection stops. Plumes appear to develop in two stages: rapid initial growth lasting until a low multiple of injection time and accounting for almost all of the difference in plume migration distance, (labeled “inflation” on Figure 5), followed by almost uniform growth insensitive to CO₂ density.

The stabilized plume configuration shown on Figure 4 is approximately elliptical in outline. Examination of similar figures for the other cases shows the same general shape. The ultimate plume areas were estimated using an elliptical approximation. Figure 6 plots the ratio of the plume area for a particular case to the PT centroid case against the ratio of the density difference between CO₂ and brine for a particular case to the PT centroid case. The relationship is almost linear. The most significant departure is at a high relative density difference (low CO₂ density). Part of this departure is likely due to grid effects, however, as the low CO₂ density plume migrated into a coarser region of the grid. Figure 6 also shows the relative plume migration distance (average for the flat cases and updip for the dipping cases) against relative density difference.

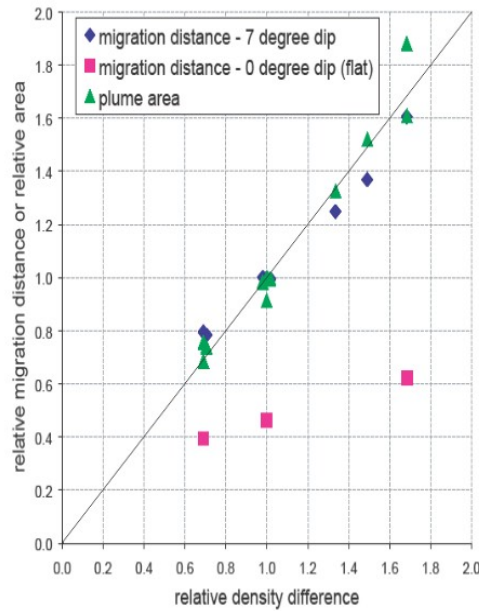


Figure 6. Ultimate CO₂ plume relative migration distance and relative area plotted against relative CO₂-brine density difference (specific case relative to centroid case).

7. Comparison to Analytical Solutions

The lack of sensitivity to brine viscosity accords with published analytical solutions for plume behavior during the injection phase. Bachu et al. [1] defined G and I as dimensionless numbers controlling plume behavior for flat reservoirs. Γ is a ratio of buoyant to viscous and pressure forces and λ is the ratio of native (brine in this case) to injected (CO₂ in this case) fluid viscosity, as follows:

$$\Gamma = \frac{2\pi\phi\Delta\rho g k k_{rb} B^2}{\mu_b Q}, \lambda = \frac{\mu_b}{\mu_{CO_2}}$$

where ϕ is porosity, $\Delta\rho$ is the fluid density difference, k is permeability, k_{rb} is the relative brine permeability, B is the aquifer thickness, μ is viscosity with subscript b for brine and CO₂ for carbon dioxide, and Q is injection rate.

According to Bachu et al. [1], when $\Gamma > 10$, buoyant forces strongly dominant, and $\Gamma*\lambda$ controls plume behavior. The brine viscosity cancels out in this product. G for the simulated cases in this study ranges from 17 to 51. While Bachu et al. [1] considered flat reservoirs, the current study suggests that the lack of sensitivity to brine viscosity for G greater than ten applies to at least shallow dipping reservoirs as well. Interestingly, linear regression on the results of the modeled cases indicates plume size correlates just as well to $\Delta\rho$ as to $\Gamma*\lambda$. This is despite the fact that $\Gamma*\lambda$ includes μ_{CO_2} as another variable that is somewhat inverse to $\Delta\rho$. The $\Gamma*\lambda$ correlation covers a range of greater than five as compared to a range of greater than two for $\Delta\rho$ alone. The correlation to $\Delta\rho$ has the added advantage of a zero intercept (direct proportionality), though.

8. Conclusions

The maximum migration distance of injected supercritical CO_2 is approximately linearly correlated to the CO_2 density uncertainty or variation resulting from PT uncertainty or in-reservoir variation. The migration distance was not found to be sensitive to brine viscosity variation, which accords with an available analytical solution [1]. For the shallow dipping case at the Kimberlina site the maximum migration distance varies by approximately a factor of two across the range of probable PTs. This has implications for risk assessment in terms of plumes intersecting potential leakage conduits such as abandoned wells or faults, and for decisions regarding storage rights acquisition for future projects.

Typically the majority of the ultimate difference in CO_2 migration distance resulting from other than expected PT conditions manifests during the injection phase. This effect provides assurance that CO_2 density deviations from project expectations can be detected early, allowing for appropriate project modification if necessary, such as remediation of abandoned wells, acquisition of more storage rights, or an increase or decrease in injection rate.

The ratio of the plume area at a particular CO_2 density relative to the area at the most probable CO_2 density is almost directly proportional to the ratio of a particular brine- CO_2 density difference relative to this difference at the most probable PT. If confirmed by future work, this affords a rule of thumb for estimating the range of possible plume sizes from a single numerical simulation and analysis of PT probability. This could provide for a rapid, first cut estimation of the storage rights necessary for a project under different PT scenarios, and for assessing CO_2 leakage risk.

The much earlier stabilization of low CO_2 density plumes in dipping strata indicates a tradeoff between storage efficiency and monitoring time. Sites supporting lower CO_2 densities will be relatively less efficient at storing CO_2 , and consequently require relatively greater storage rights acquisition, but they will require shorter monitoring times. However, the driving forces and potential for leakage will be greater at lower CO_2 density sites. Combining the downsides of the greater leakage risk with the need for relatively more storage rights supports the conventional wisdom that sites affording high CO_2 density are probably more economically efficient.

This study motivates some questions for further research. How does the PT range observed in subbasins scale to single storage reservoirs? Does observed distribution of PT-depth gradients derive from measurement uncertainty and/or actual variation in the subsurface? Do current and planned CO_2 injections (including pilot tests) have a systematically higher Γ than will industrial injections? If they do, does this pose a problem for applying results of these projects to future projects? For instance, will different phenomena occur that are significant in terms of capacity utilization or risk profile? If so, is it yet possible to design a pilot test program around the relevant range of Γ ?

Acknowledgments

We are grateful to Jeff Wagoner (LLNL) for sharing his expertise regarding the geology of the southern San Joaquin Valley, particularly in the vicinity of the Kimberlina site, and Curt Oldenburg for his review leading to its improvement, including implications for risk. This work was supported in part by the CO₂ Capture Project (CCP) of the Joint Industry Program (JIP), by WESTCARB through the Assistant Secretary for Fossil Energy, Office of Sequestration, Hydrogen, and Clean Coal Fuels, National Energy Technology Laboratory (NETL), and by Lawrence Berkeley National Laboratory under U.S. Department of Energy Contract No. DE-AC02-05CH11231.

References

1. S. Bachu, J.M. Nordbotten, and M.A. Celia, Evaluation of the spread of acid gas plumes injected in deep saline aquifers in western Canada as an analogue for CO₂ injection in continental sedimentary basins, *Greenhouse Gas Control Technologies* 7, Proceedings of the 7th International Conference on Greenhouse Gas Control Technologies 5– September 2004, Vancouver, Canada 2005 edited by: E.S. Rubin, D.W. Keith, C.F. Gilboy, 479–487.
2. California Department of Conservation, Division of Oil, Gas and Geothermal Resources, *California Oil and Gas Fields*, Volume 1, Sacramento, California, 1998.
3. K. Pruess, C.M. Oldenburg, and G. Moridis, TOUGH2 user's guide, version 2.0, Rep. LBNL-43134, Berkeley: Lawrence Berkeley National Laboratory, 1999.
4. K. Pruess and J. García J (2002) Multiphase flow dynamics during CO₂ disposal into saline aquifers. *Environmental Geology* 42: 282–295
5. C. Doughty, Modeling geologic storage of carbon dioxide: comparison of hysteretic and non-hysteretic characteristic curves, *Energy Conversion and Management* No. 48 (2007) 1768–1781.